In Vivo Quantification of Retraction Deformation Modeling for Updated Image-Guidance During Neurosurgery

Leah A. Platenik, Michael I. Miga, David W. Roberts, Karen E. Lunn, Francis E. Kennedy, Alex Hartov, and Keith D. Paulsen*, *Member, IEEE*

***Abstract*—The use of coregistered preoperative anatomical scans to provide navigational information in the operating room has greatly benefited the field of neurosurgery. Nonetheless, it has been widely acknowledged that significant errors between the operating field and the preoperative images are generated as surgery progresses. Quantification of tissue shift can be accomplished with volumetric intraoperative imaging; however, more functional, lower cost alternative solutions to this challenge are desirable. We are developing the strategy of exploiting a computational model driven by sparse data obtained from intraoperative ultrasound and cortical surface tracking to warp preoperative images to reflect the current state of the operating field. This paper presents an initial quantification of the predictive capability of the current model to computationally capture tissue deformation during retraction in the porcine brain. Performance validation is achieved through comparisons of displacement and pressure predictions to experimental measurements obtained from computed tomographic images and pressure sensor recordings. Group results are based upon a generalized set of boundary conditions for four subjects that, on average, account for at least 75% of tissue motion generated during interhemispheric retraction. Individualized boundary conditions can improve the degree of data-model match by 10% or more but warrant further study. Overall, the level of quantitative agreement achieved in these experiments is encouraging for updating preoperative images to reflect tissue deformation resulting from retraction, especially since model improvements are likely as a result of the intraoperative constraints that can be applied through sparse data collection.**

***Index Terms*—Image-guided neurosurgery, retraction, subsurface deformation model.**

Manuscript received July 9, 2001; revised March 18, 2002. This work was supported by the National Institutes of Health (NIH) under National Institute of Neurological Disorders and Stroke Grant R01-NS33900. *Asterisk indicates corresponding author.*

L. A. Platenik, K. E. Lunn, and F. E. Kennedy are with the Thayer School of Engineering, Dartmouth College, Hanover, NH 03755 USA.

M. I. Miga is with the Department of Biomedical Engineering, Vanderbilt University, Nashville, TN 37069 USA.

D. W. Roberts is with Dartmouth Hitchcock Medical Center, Lebanon, NH 03766. He is also with the Norris Cotton Cancer Center, Lebanon, NH 03766 USA.

A. Hartov is with the Thayer School of Engineering, Dartmouth College, Hanover, NH 03755. He is also with Dartmouth Hitchcock Medical Center, Lebanon, NH 03766 USA.

*K. D. Paulsen is with the Thayer School of Engineering, Dartmouth College, 8000 Cummings Hall, Hanover, NH 03755-8000 USA. He is also with Dartmouth Hitchcock Medical Center, Lebanon, NH 03766 USA, and the Norris Cotton Cancer Center, Lebanon, NH 03766 USA (e-mail: keith.d.paulsen@dartmouth.edu).

Publisher Item Identifier 10.1109/TBME.2002.800760.

I. Introduction

THE REGISTRATION of case-specific preoperative images to patient and instrument locations in the operating room (OR) [1]–[8] may be inadequate for image guidance due to brain deformation which occurs concurrent with surgery. The extent of intraoperative brain shift has been documented in several recent studies [9]–[14]. These reports indicate that the fidelity of preoperative-based image guidance can be significantly compromised and suggest that a new generation of adaptive image-guided systems are needed; of which, intraoperative magnetic resonance (iMR) has emerged as an attractive option. While the ability to perform whole-volume imaging during surgery is appealing; iMR is potentially disruptive to traditional OR protocol and not necessarily amenable to updating all forms of preoperative data [e.g., functional magnetic resonance imaging (fMRI), single photon emission computed tomography (SPECT), positron emission tomography (PET), etc.] that might be important to clinical decision making in the OR without additional image processing [15]. Another possible strategy for achieving dynamic image-guidance was recently described by Roberts *et al.* [16] and could serve to complement iMR or perhaps eliminate the need for whole-volume imaging in the OR during many procedures. In this approach, computational models of brain biomechanics are used in conjunction with intraoperative data acquisition to provide a three-dimensional (3-D) nonrigid volumetric transformation for all image data. As a complement to iMR, this scheme could be used to generate interscan updates or to compensate for out-of-field deformation during intraoperatively acquired single-plane or partial-volume imaging.

Several groups have investigated the potential value of physical models in this context and have pursued related ideas which are underpinned by biomechanical concepts [17]–[21]. The advantage of modeling is the ability to incorporate the physical and structural properties of tissue preoperatively (e.g., through magnetis resonance elastography and diffusion tensor imaging) in combination with knowledge of the mechanical influences imposed on the brain during surgery. Initial work was two-dimensional [17], [19], [22] but quickly progressed to 3-D in terms of both lumped element [18] and continuum mechanical [20] realizations. While significant advances have been reported, issues pertaining to fast processing [23], [24] and biophysical constituitive laws [25] remain as important areas of investigation.

The challenge in the modeling approach is to develop a computationally tractable framework that is advanced enough to

translate complex intrasurgical events into sufficiently accurate estimates of tissue mechanical response which can be used to maintain image-to-patient correspondence throughout surgery. Toward this end, we have implemented a 3-D biphasic computational prescription of brain deformation based on consolidation physics and have begun the process of both extending our ability to model increasingly invasive neurosurgical interventions and validating *in vivo* the accuracy of resulting deformation estimates in animal and human systems. In previous work, we have evaluated model predictions of detailed tissue displacement maps and pressure fields induced in the porcine brain by uni-axial piston translation and balloon catheter inflation [26], [27]. Initial modeling attempts in humans have focused on capturing brain shift due to gravitational sag which has been found to be a significant component of tissue motion in the OR. In all of the studies, model predictions have compensated for nearly 80% of the brain deformation observed which has been encouraging and represents a major step forward relative to navigating with preoperative image to OR field registration. More recently, we have reported computational strategies for estimating displacement due to both tissue retraction and resection and demonstrated their successful employment in a clinical case study, although no quantitative validation has been undertaken to date [28].

The goal of this paper is to provide the first quantitative assessment of our tissue retraction model using the porcine brain system. Specifically, we develop a new incremental formulation for model deployment which is important during retraction where, unlike previous uni-directional piston experiments, the loading conditions possess a directional dependency that varies incrementally over time. In addition, we report on the use of more generalized boundary conditions for the hydrodynamic component of the model at the retractor site which involve transport coupling coefficients that provide anti-symmetrical pressure responses across the retraction boundary—behavior which again is more complex than that encountered during previous pig experiments. Overall, the results are encouraging and demonstrate through detailed comparisons between experiments and model predictions that the model-driven updates can compensate for approximately 80% of the induced tissue motion during retraction.

II. Materials and Methods

A. Computational Model and Mesh Generation

The field equations for the tissue model we are using can be written as

$$\nabla \cdot G\nabla \mathbf{u} + \nabla \frac{G}{1-2\nu}(\nabla \cdot \mathbf{u}) - \alpha \nabla p = \mathbf{F} \tag{1a}$$

$$\alpha \frac{\partial}{\partial t}(\nabla \cdot \mathbf{u}) + \frac{1}{S}\frac{\partial p}{\partial t} - \nabla \cdot k\nabla p = \Psi/S \tag{1b}$$

where

- $\mathbf{F}$ force/unit volume (N/m^3);
- Ψ pressure source strength (Pa/s);
- G shear modulus (Pa);
- ν Poisson's ratio;
- $\mathbf{u}$ displacement vector (m);
- p pore fluid pressure (Pa);
- α ratio of fluid volume extracted to volume change of the tissue under compression;
- k hydraulic conductivity ($\mathrm{m}^3\mathrm{s/kg}$);
- $1/S$ amount of fluid which can be forced into the tissue under constant volume ($1/Pa$).

There is a growing literature on low impact biomechanics of the brain (e.g., [20], [25], and [29]–[31], among others) despite the fact that historically brain tissue mechanical response during surgery has received modest attention. Equations (1a) and (1b) were originally developed by Biot [32] in the 1940s for soil mechanics but have been recently adapted and applied to the brain [29], [30], [33]. This model is attractive because of its linear (i.e., computationally efficient with a small number of physically motivated tissue property parameters) multi-phasic (i.e., recognizes the important influence of the hydrodynamical component of the brain) character which mimics the porous media response of a sponge—an intuitive approximation argued on biophysical principles by Hakim [34]. However, it also has clear limitations [35], for example, it does not explicitly include the vascular compartment within the brain or account for the viscoelastic behavior of retracted tissue over time scales relevant to surgery (e.g., see [28]). In fact, an important element of the effort reported here is the degree to which the approximations of brain deformation from surgical loading embodied in this consolidation model hold up *in vivo*.

In previous numerical implementations of this computational framework (e.g., [33]), a linear formulation of the consolidation equations has been employed in terms of total field variables. Following the weighted residual treatment of (1a) and (1b), the continuum equations can be converted into discrete matrix form

$$[K_o]\mathbf{x} = r \tag{2}$$

where $[K_o]$ is the stiffness matrix, $\mathbf{x} = \{u_1, v_1, w_1, p_1, u_2, v_2, w_2, p_2, \ldots u_n, v_n, w_n, p_n\}$ with u, v, w, and p representing the calculated cartesian (total field) displacement and pressure, and r is a collection of known boundary and body force conditions. To achieve the complete solution to a series of successive surgically induced deformations, this translates into continuous modification of the boundary condition data in order to represent the entire history of surgical events. The formulation has the advantage that the solution has no path dependence (i.e., is order-independent). However, extrapolation to large-strain mechanics or trajectory dependent deformation cannot be accomplished with this approach, of which, the latter becomes important when modeling surgical retraction.

As a result, we have altered our current strategy to accommodate an incremental formulation

$$[K_i](\delta \mathbf{x_i}) = (\delta r_i). \tag{3}$$

In this treatment, a series of solutions experiencing incremental strains is combined to determine the total displacement and pressure throughout the domain, i.e.,

$$\mathbf{u_{i+1}} = \mathbf{u_i} + \delta \mathbf{u_i} \tag{4a}$$

$$p_{i+1} = p_i + \delta p_i \tag{4b}$$

with $\mathbf{u_o}$ and p_o being the initial state. To strictly follow this incremental strategy and account for geometric nonlinearities, the computational domain would need to be repetitively deformed to reflect its new state at each step. However, one strategy to alleviate the computational overhead associated with re-meshing is to use the original stiffness matrix from the initial state at each

increment, i.e., $[K_n] = [K_{n-1}] = \cdots = [K_o]$. Hence, we assemble a single stiffness matrix on the undeformed mesh as in (2) and use these coefficients to repeatedly solve (3) for each increment of applied forcing (here, each retraction increment as described in Section II-C). Although this leads to a departure from the true-path loading, the approach maintains computational tractability; and we have found that the modification to computing incremental field variables increases the fidelity of our model-based technique [36]. While the linear incremental strategy is an improvement, it is also important to recognize that it does not necessarily yield the same solution as modeling the nonlinear mathematics associated with large deformation mechanics.

B. Retraction Technique and Boundary Condition Description

Although the retraction of brain tissue during surgery is common, detailed studies on the effects of retraction on tissue are few [37]. The simulations that do exist are largely concerned with realistic visual behavior for surgical simulation [38] and are not intending to produce accurate force/stress estimation in an effort to understand the mechanical impact on the parenchyma. We have recently presented a strategy to accurately reflect the effects of retraction on tissue which maintains computational tractability with the potential of providing intraoperative feedback to the surgeon [28]. While our methods have not been optimized to conserve compute time (current updates require on the order of tens of minutes), near-real-time intraoperative image processing and updating will likely be important and schemes which do achieve refresh rates on the order of tens of seconds using parallel computing have been demonstrated [23], [24].

Our approach begins with the generation of a computational mesh of the subject's brain using preoperative images (CT or MR) manipulated through AnalyzeAVW[1] . The boundary is discretized into triangular patches using the marching cubes algorithm. Custom mesh generation software creates a volumetric mesh with tetrahedral elements [39], having increased discretization in the region of surgical focus. (All meshes in this study contained at least 19 000 nodes, resulting in minimal discretization errors with total displacement variances below 0.1 mm [26].)

In the experiments reported here, the area of focus was located along the superior midline of the pig brain, resulting in the geometric coincidence of fissure and retractor. A plane describing the position and orientation of the retractor and interhemispheric fissure was determined using baseline CT scans or, when necessary, a coregistered pre-operative MR series of the corresponding subject. The plane was incorporated into the mesh using a splitting technique for retraction described by Miga *et al*. [28]. Unit vectors extending from the centroids of intersecting tetrahedral elements to the closest patch on the retractor plane are determined to be either positive or negative with respect to the direction normal to the fissure or the direction of retraction. For each transected elemental vertice, a coincident node is created and moved a distance equal to the width of the retractor in the direction of its surface normal.

[1]AnalyzeAVW v3.1-Biomedical Imaging Resource, Mayo Foundation, Rochester, MN. Software was provided in collaboration with the Mayo Foundation. Codman Microsensor ICP Transducers were donated by Johnson & Johnson.

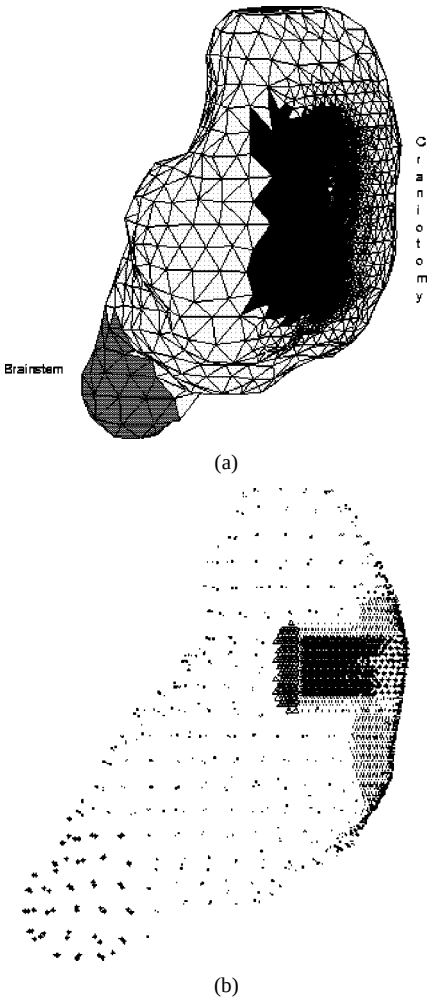

Fig. 1. Graphical illustration of boundary conditions. (a) Cut-away view of the craniotomy and shaded region associated with the brain stem. (b) Model zones associated with the removal of the dura and the placement of the retractor.

The new nodes define an additional surface representing tissue parallel to the duplicated surface, creating a fissure and providing two independent degrees of freedom corresponding to the tissue on either side of the retractor. In all subjects, the interhemispheric surface of the left hemisphere was in virtual contact with the compressive, front side of the retractor, while the right hemisphere was initially in virtual contact with the space-creating, back side of the retractor.

A pictorial representation of the distribution of boundary conditions for a typical model is shown in Fig. 1. Fig. 1(a) is a surface mesh description that includes a cut-away view of the craniotomy while Fig. 1(b) illustrates various zones within the model which support different boundary data. In the region of the craniotomy where the dura was removed [superior dense section of points in Fig. 1(b)] as well as in the modeled fissure, stress-free conditions have been prescribed with no drainage. The surface in contact with the retractor front [dark, superior to inferior directed subsection in Fig. 1(b)] was prescribed to move a known displacement in a direction normal to the retractor blade which was measured from intraoperative CT data. In these measurements, the compliance in our deformation delivery system (retractor blade translation assembly, see Section II-C) caused small changes in its trajectory from increment to increment.

The advantage of the formulation in equation (3) is that the application of model boundary conditions can be altered incrementally to more accurately describe the measured deformation trajectory. We have found this subtle adjustment improves our ability to predict the deformation path development in our experimental system [36]. On the retractor back (not shown in Fig. 1), we have specified that the tissue displaces with the retractor during its early movements and subsequently separates at larger retractions which was empirically evident in the intraoperative CT data. The cause of this behavior is not completely clear but may result from some initial blood clotting which loosely binds the tissue to the retractor during the initial stages or from a tearing of the tissue inferior to the retractor at increased retraction, freeing the opposite hemisphere. It is also the case that tissue under normal conditions experiences an internal pressure which is released upon separation from its surroundings which may account for the observed motion by allowance for some expansion into the void created by retraction.

In recent work by Miga *et al.* [26], a mixed boundary condition relating subarachnoid pressure to interstitial pressure was provided for far-field drainage conditions. In this work, a similar boundary condition is applied which relates the communication of pressure immediately under the retractor, p_r, to the adjacent interstitial fluid in the tissue by a transport coupling coefficient, k_r, and is written

$$\frac{\partial p}{\partial n} = k_r(p - p_r). \tag{5}$$

As with displacement, the conditions for pressure are equal but opposite in sign on the front and back sides of the retractor for initial deformation increments, while pressure is decreased for subsequent deformations. In previous work [27], [26] a boundary calibration curve relating pressure to applied deformation was directly enforced which did not allow for strain-induced pressure rises immediately under the deformation source. In regions outside the craniotomy [sparsely dotted areas distal from the retractor location in Fig. 1(b)], the tissue has been allowed to slip along the cranial cavity with no drainage specified. The pressure in the brain stem area [darker, but less dense dotted area inferior to the craniotomy in Fig. 1(b)] was assigned to be zero to reflect conditions associated with herniation observed in this region of the human brain. Tissue properties used in the model are similar to those we have employed in previous studies ($G = 1027\ Pa$; $\nu = 0.46$; $k = 1.0$ E-11 m^{3}s/kg).

C. In Vivo Experimental Procedures

To measure controlled surgical displacements, the experimental porcine protocol developed previously and described by Miga *et al.* [26], [27] was used as the foundation for the procedures employed in this study. Following anesthesia, a craniotomy was performed approximately centered both medial and anterior/posterior, leaving the dura temporarily intact. Four subjects weighing 34–45 lbs., were involved. All procedures were approved by the Institutional Animal Care and Use Committee at Dartmouth College. Using a 14 gauge needle, 20–22 stainless-steel beads (1-mm diameter) were implanted into the parenchyma near the interhemispheric fissure in a grid-like fashion using fluoroscopic imaging for guidance. Fixation of the beads in the tissue was determined by fluoroscopic examination performed intermittently throughout the implantation procedure, as illustrated in Fig. 2(a). The exposed dura on the hemisphere designated for retraction was carefully removed. A retractor was inserted into the hemispheric fissure, in line with the grid of beads. The retractor was then mounted to the stereotactic frame holding the subject [see Fig. 2(b)]. The apparatus allowed for unidirectional translation of the retractor laterally away from the midline by rotating a calibrated lead-screw mechanism. Acquisition of a baseline CT scan (0.3 mm $\times$ 0.3 mm $\times$ 1 mm) was taken prior to successive translations (3, 6, 8, and, optionally, 10 mm) of the mounted retractor. Registration was provided by the stereotactic frame, thus allowing detailed spatial trajectories for all implanted beads to be recorded. Interstitial pressure was also recorded in both hemispheres with an invasive probe (Johnson & Johnson Codman Microsensor ICP Transducers) inserted directly into

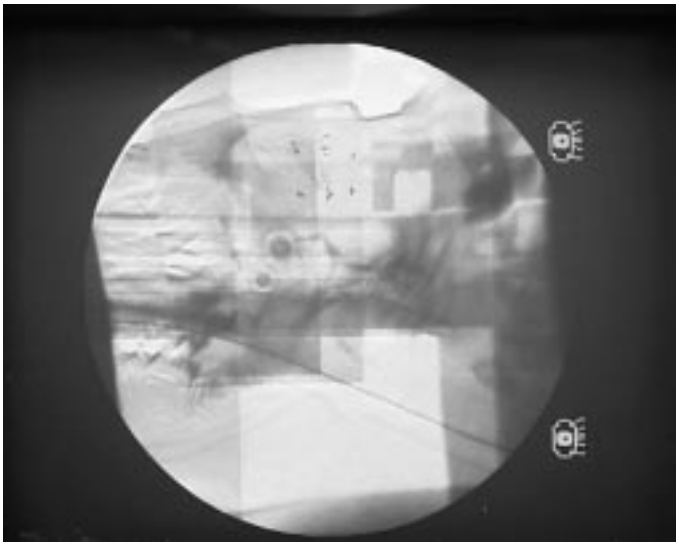

(a)

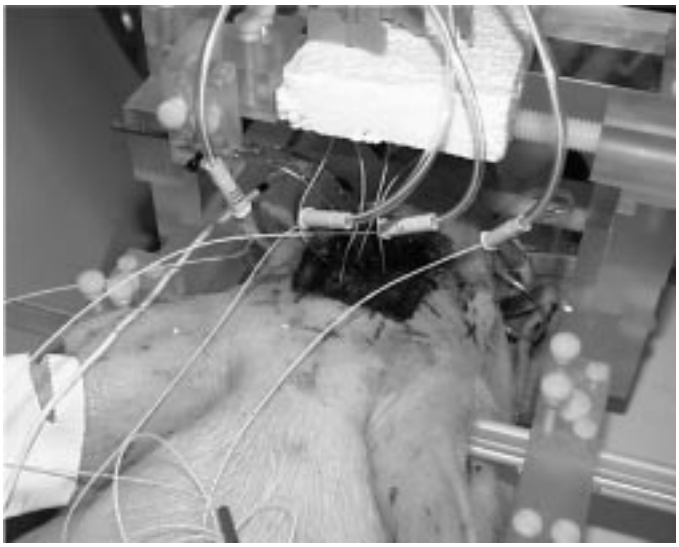

(b)

Fig. 2. Procedures used during the *in vivo* porcine experiments. (a) Fluoroscopic image of marker locations in the parenchyma. (b) Interhemispheric retractor attached to the translation system integrated into the stereotactic frame holding the subject. The placement of pressure sensor probes directly into the parenchyma can be seen.

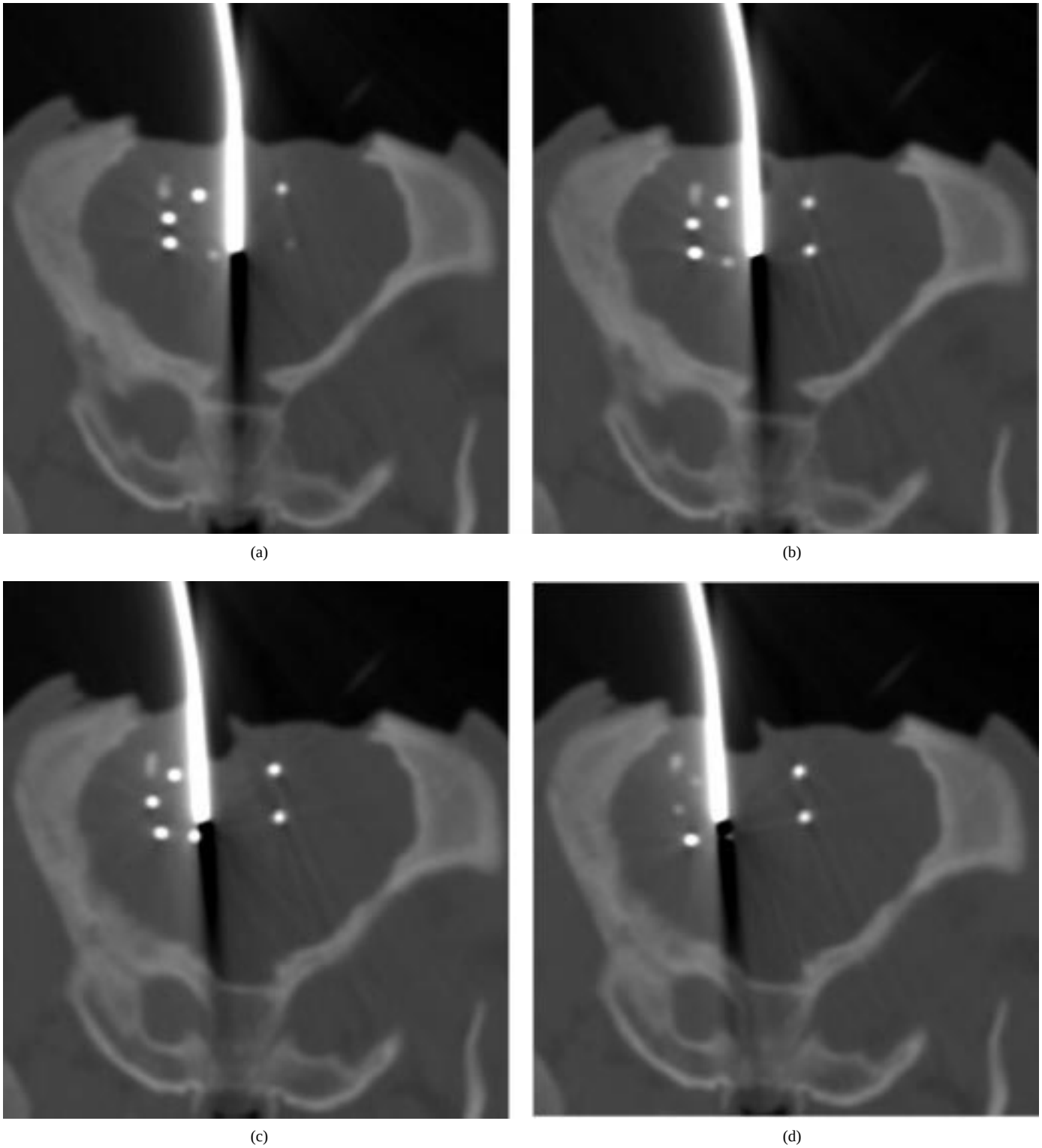

Fig. 3. Anatomically coronal CT scans of incremental retraction. (a) Baseline. (b) Step 1): 3 mm. (c) Step 2): 6 mm. (d) Step 3): 8 mm.

the parenchyma in two of the four experiments as illustrated in Fig. 2(b).

III. Results

We have organized our presentation of the results into three subsections. Because of the relatively large amount of data (four subjects, three to four retractions/subject, 20–22 beads/subject), we have summarized model comparisons in terms of average and maximum error metrics across subjects for each retraction. However, it is also informative to examine the spatial details of the data-model match in an individual subject. As a result, in the first subsection we report the experimental data predominantly in averaged form, then in the second subsection quantify specific comparisons between model calculations and measured quantities for a single subject and conclude with the third subsection

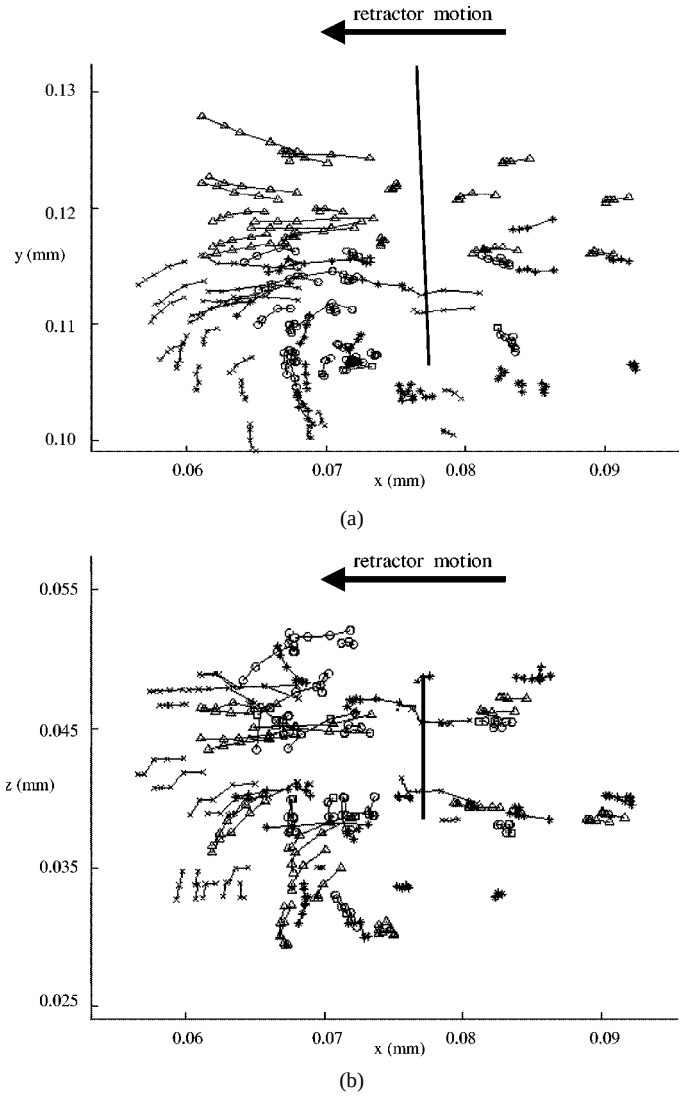

Fig. 4. Bead trajectory comparison across subjects. x: Subject 1. o: Subject 2. $\triangle$: Subject 3. $*$: Subject 4. (a) Coronal view (X–Y plane). (b) Axial view (X–Z plane). The initial retractor position is represented by the solid line in each plane and the direction of retraction is shown.

which reports summary data across the animal group used in the study.

A. Experimental Data

Fig. 3 shows a typical sequence of CT scans illustrating bead movements created during a series of retraction steps. The movement of the blade, brain parenchyma and implanted beads in the retracted hemisphere is clearly evident compared to the relatively modest motion of the beads visible in the contralateral side. Fig. 4 presents orthogonal views of bead trajectories across all four subjects. While each experiment contains elements of displacement that exhibit individual characteristics, the overall deformation fields are reasonably similar within the four brains despite some differences in brain volume and retractor placement. Specifically, there is an overall preference for posterior and inferior movement (i.e., toward the brain stem) secondary to the dominant lateral displacement in the retraction direction for many of the beads, although there is some anterior/superior motion in a few isolated instances.

TABLE I
MEASURED RETRACTOR DISPLACEMENTS: TOTAL AND INCREMENTAL (INC) IN MILLIMETERS FOR EACH SUBJECT

Retraction Step No.	Subject #1 total (inc)	Subject #2 total (inc)	Subject #3 total (inc)	Subject #4 total (inc)	Average total (inc)
1	3.5	2.7	3.2	3.2	3.2
2	7.4 (3.9)	6.0 (3.3)	6.4 (3.2)	6.1 (2.9)	6.5 (3.3)
3	9.5 (2.1)	8.0 (2.0)	8.2 (1.8)	8.2 (2.1)	8.5 (2.0)
4	11.6 (2.1)	na	9.9 (1.7)	na	10.4 (1.9)

TABLE II
AVERAGE AND MAX MEASURED BEAD DISPLACEMENTS: MAGNITUDE (U) AND $x(U_x)$, $y(U_y)$ AND $z(U_z)$ DIRECTIONAL COMPONENTS IN MILLIMETERS FOR ALL FOUR SUBJECTS. STANDARD DEVIATIONS ($\pm$) ARE ALSO REPORTED FOR AVERAGED RESULTS

Retraction Step No.	U_x (mm) Average (Max)	U_y (mm) Average (Max)	U_z (mm) Average (Max)	U (mm) Average (Max)
1	0.9±0.8 (2.7)	0.3±0.3 (1.1)	0.4±0.4 (1.2)	1.2±0.7 (2.9)
2	1.7±1.5 (5.5)	0.7±0.5 (2.5)	0.7±0.7 (2.5)	2.3±1.3 (5.5)
3	2.1±1.9 (7.4)	0.9±0.7 (3.0)	0.9±0.3 (3.3)	2.8±1.7 (7.4)
4	3.0±2.4 (8.5)	1.0±0.8 (3.0)	1.2±1.1 (3.9)	3.8±2.2 (8.5)

Reported in Table I is the measured blade movement for each retraction event for all four subjects. Two subjects underwent a series of three retractions while the remaining two subjects experienced a fourth retraction; therefore, averaged results are based on a sample of $n = 4$ for retraction steps 1)–3) and $n = 2$ for retraction Step 4. Both the accumulated total and incremental distances the blade moved are tabulated. Table II contains the average and standard deviation in the bead displacements in terms of total magnitude and Cartesian directional components for each retraction step across the subject pool. Although the mounted translational apparatus was designed to be unidirectional, slippage in linked components and the retractor's inherent flexibility resulted in slightly angled displacements of the blade. Even so, the majority of displacement occurred in the nominal retraction or x direction with smaller movements recorded in the y and z directional displacements between subjects.

B. Individual Subject Comparisons

Fig. 5 shows comparisons of measured and computed bead locations presented in orthogonal views for Subject 3. The complete trajectories from all four retractions are included. It is important to analyze individual bead errors for a given retraction to determine the degree to which the model correctly estimates the local deformation field. Fig. 6 reports measured and computed bead displacement as a function of bead number for the second retraction in this same subject. It compares not only measured and computed values of total displacement magnitude but

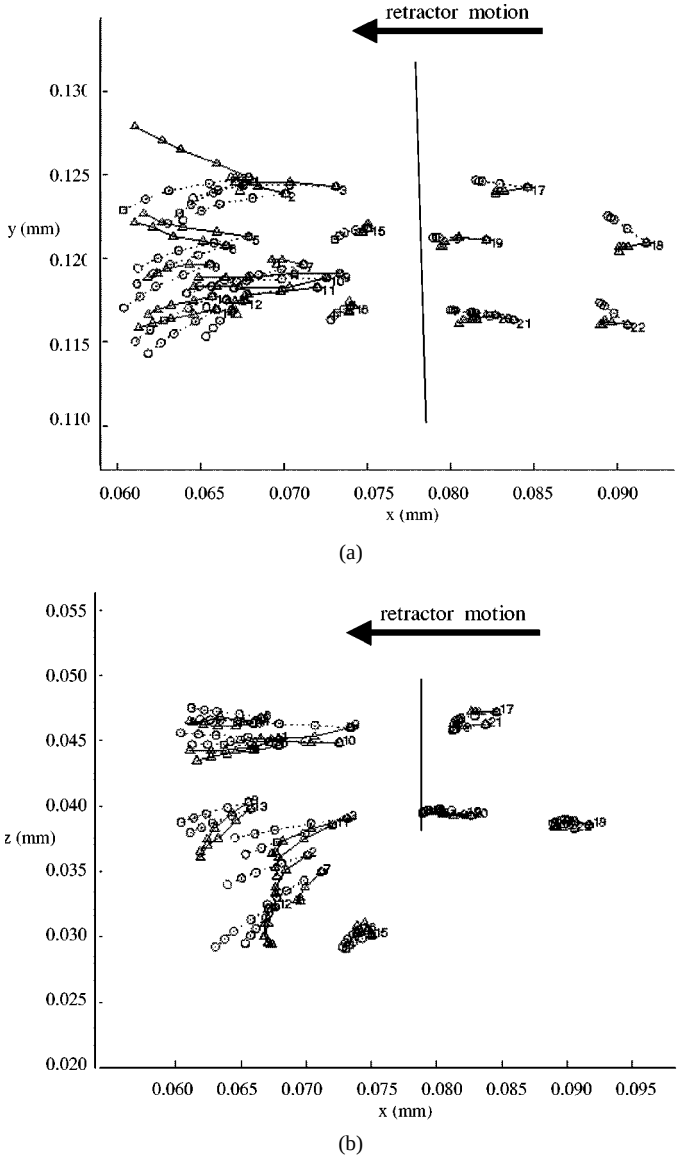

Fig. 5. Subject 3 comparison between measured and calculated bead trajectories. △-measured. o: calculated. (a) Coronal view (X–Y plane), (b) axial view (X–Y plane). The initial retractor position is represented by the solid line in each plane and the direction of retraction is shown.

also the three directional (Cartesian) components of the deformation at each bead location. The error in displacement magnitude and the magnitude of the difference error vector are also shown in order to gauge both the size and directional quality of the match between measured and computed motion. The model also has a hydrodynamical component and pressure fields can be compared in Subject 3 as well. Fig. 7 shows the pressure traces recorded during this experiment along with their computed counterparts.

Given some appearance of systematic differences in the experimental versus computed displacements in Fig. 6 (e.g., overpredictions in x, opposite direction in y), it is tempting to consider boundary conditions specific to an individual experiment in order to investigate whether these discrepancies can be eliminated. Fig. 8 shows the analogous comparison to Fig. 6 for such a case. In the latter figure, nodes representing tissue at the edges of the craniotomy in the retracted hemisphere were constrained to slip only along the edge direction. Specifically, nodes on the craniotomy edges parallel to the retraction direction were free to move in that direction whereas nodes on the edge normal to the direction of retraction were free to move parallel to that edge. In addition, tissue next to the walls of the cranium just above the brainstem were not allowed to move inferiorly nor laterally to simulate the gradual curvature of the skull confining this region near the base of the brain. These constraints were added based on empirical observations of the tissue behavior measured during bead movement in the CT-scans. While physically reasonable, they have not been supported by independent validation nor were they found to generalize effectively across the full set of experiments reported here.

C. Group Comparisons

Table III reports the average and maximum differences in the experimental and calculated displacement vectors for each retraction event for all subjects in the study. The data is presented in terms of average and standard deviation in the Cartesian directional and total magnitude error components. These errors accumulate with each retraction, however, it is possible to assess an individual retraction increment by comparing with the known location of the bead at the start of a specific retraction event. Per event differences are recorded in Table IV and indicate that the errors associated with any given retraction increment are similar, being approximately 0.2–0.3 mm. In terms of percentage errors or percent recapture of tissue motion, Table III can be recast in the form of Table V by subtracting the average relative error in each direction or total magnitude from 100 percent. The Table V measures are the same as we have used in the past [40] to quantify the overall model performance from the perspective of recovering tissue motion for updating preoperative images intraoperatively during image-guided neurosurgery.

IV. Discussion

Figs. 4–7 indicate that we can acquire a large amount of detailed information on tissue motion due to retraction using our bead tracking technique. This provides a rich environment for comparing model calculations with measured displacements *in vivo*. We have attempted to distill the large amount of data into summary form by reporting tables of average and maximum measures of tissue response and model performance while at the same time reporting representative details from individual experiments which are important for highlighting the spatial characteristics of the model-data comparisons. The results demonstrate that the model quantitatively captures the overall brain deformation behavior during retraction. The percent recapture figures of merit in Table V report a rate of 75%–80% which is quite similar to those observed in previous experiments that exploited simpler, less surgically realistic deformation sources (e.g., unilateral piston translation [26]). This is encouraging given the more complex challenges associated with modeling of tissue retraction; however, it is also clear that there is room for additional improvement.

The individual subject comparison shown in Figs. 6 and 8 reveal that the majority of the bead errors are less than 1mm, although there are some consistent discrepancies. For example, the y displacements either show little movement or are predominantly positive experimentally indicating a tendency

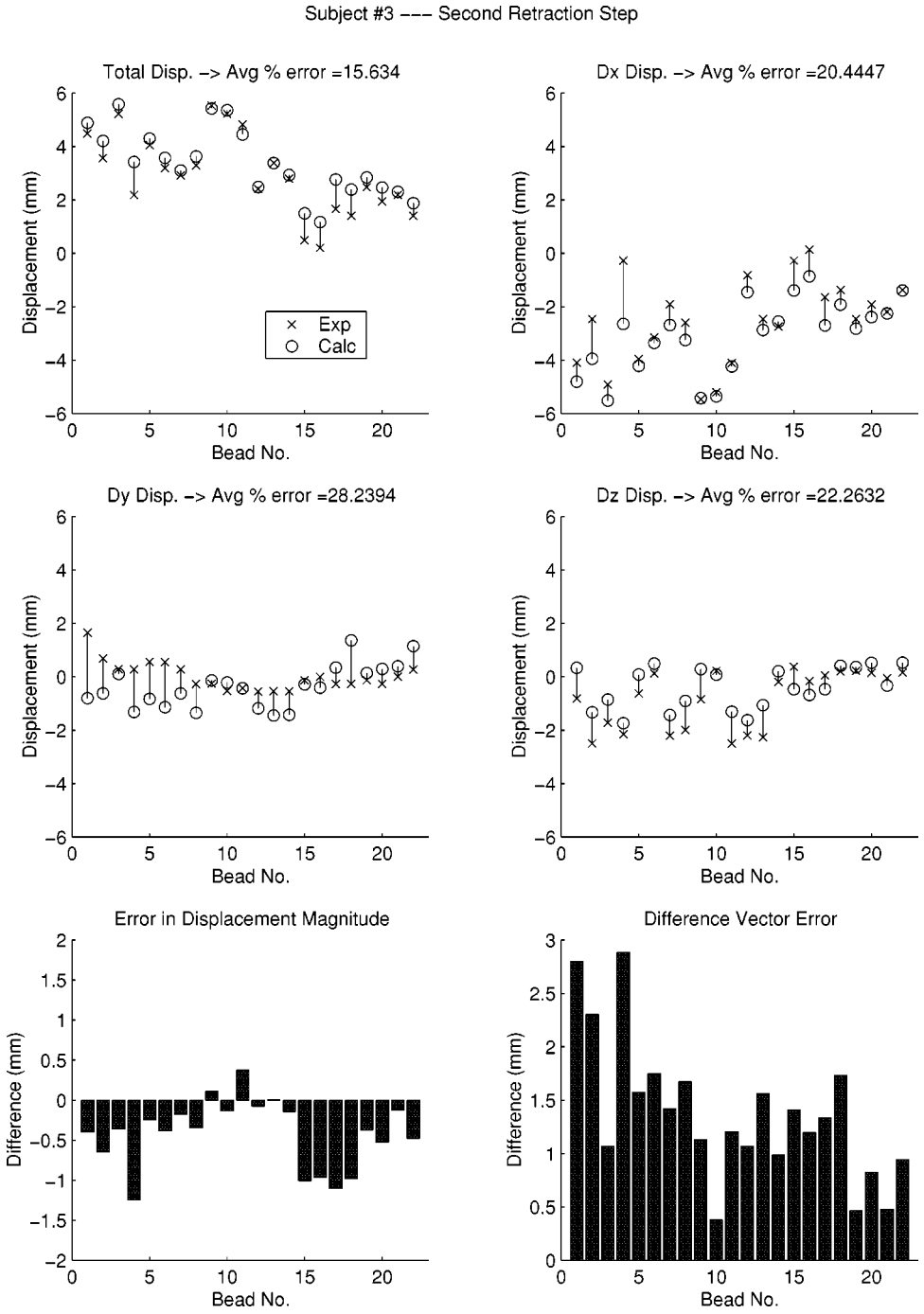

Fig. 6. Comparison of measured and computed bead displacements during the second retraction event for Subject 3 using the general boundary conditions. Total displacement magnitude (top row, left), x displacement (top row, right), y displacement (middle row, left) and z displacement (middle row, right) comparisons are shown for each bead location. The average percent errors relative to the mean displacement in total magnitude, x displacement, y displacement and z displacement are 15%, 20%, 28%, and 22%, respectively. The error in displacement magnitude (bottom row, left) and the magnitude of the difference error vector (bottom row, right) are also shown on a per bead basis.

for the beads to move superiorly during retraction whereas they move inferiorly (downward) in the model for the most part. The anterior/posterior (i.e., z displacement) motion is generally consistent between the model and the measurements; however, the model underpredicts the degree of overall movement observed experimentally. The majority of beads follow closely their x trajectories in the model relative to reality with one or two exceptions (e.g., bead 4). Interestingly, the model tends to overpredict this movement which is in the primary direction of retraction in almost every case.

Subject specific boundary conditions (e.g., Fig. 8) can improve the degree of data-model match by as much as 10% or more. In the particular case illustrated here, all components of the error vector improve with the most dramatic gains occurring in the x and y directions. For example, beads 2 and 4 in the x (retraction) direction are notably improved in Fig. 8. Complete analysis

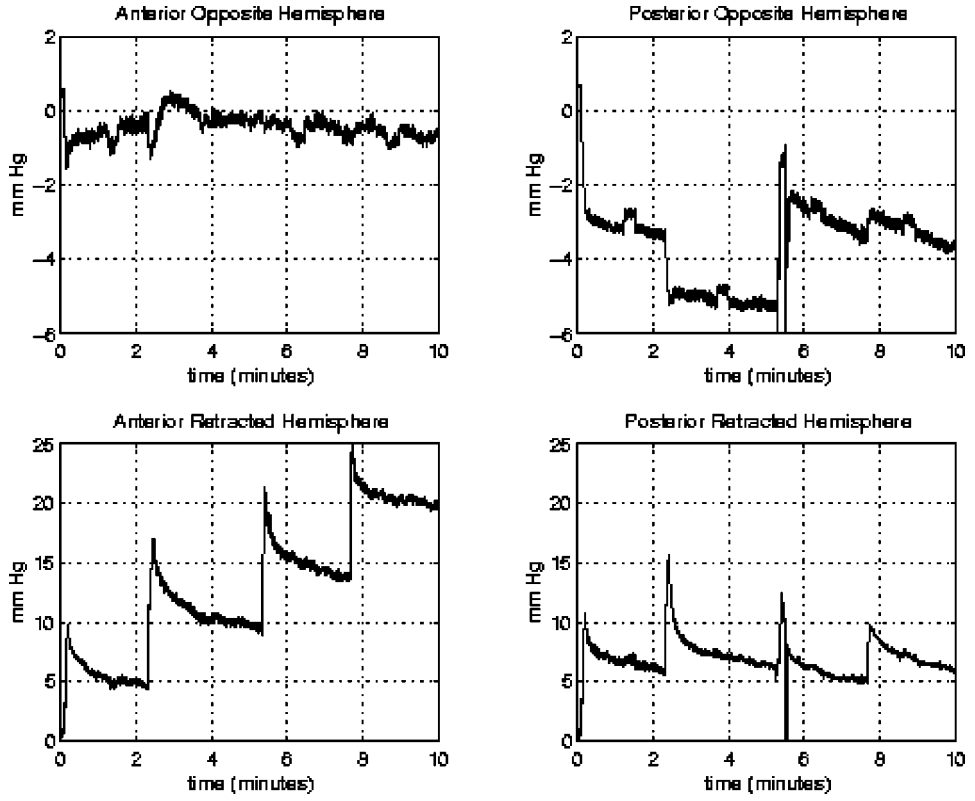

(a)

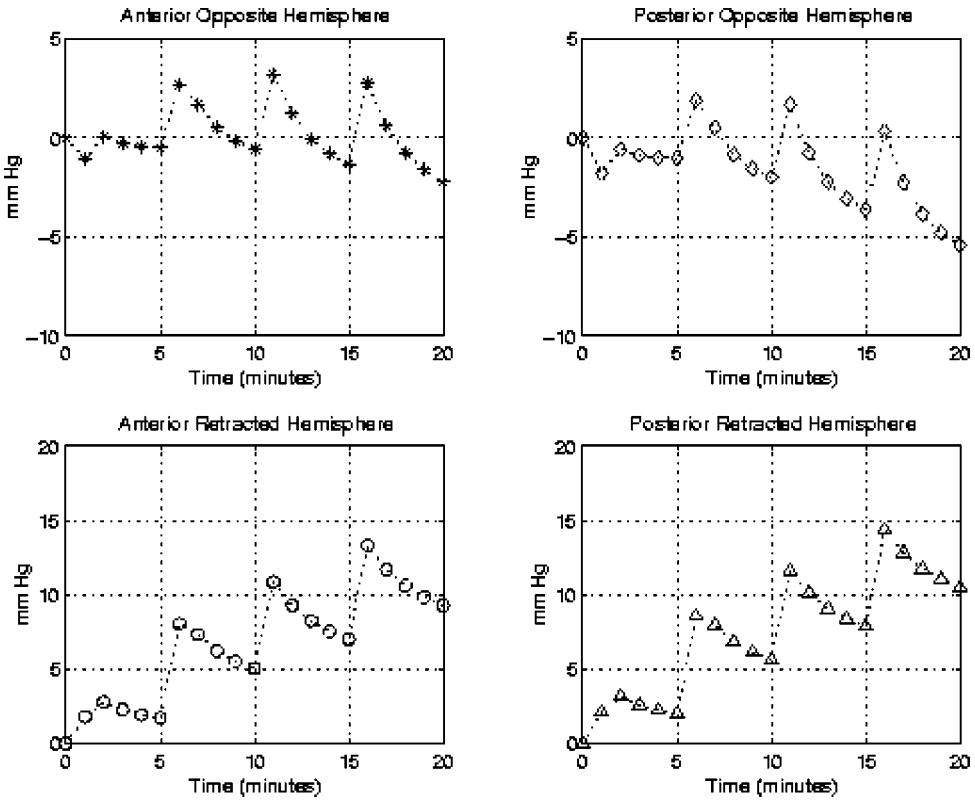

(b)

Fig. 7. Pressure data for Subject 3. (a) Experimentally measured pressure. (b) Calculated pressure.

of subject-specific boundary condition results (not shown), in terms of the percent recapture of deformation measure reported in Table V, shows that the lower bound generally improves to better than 85% of the total motion.

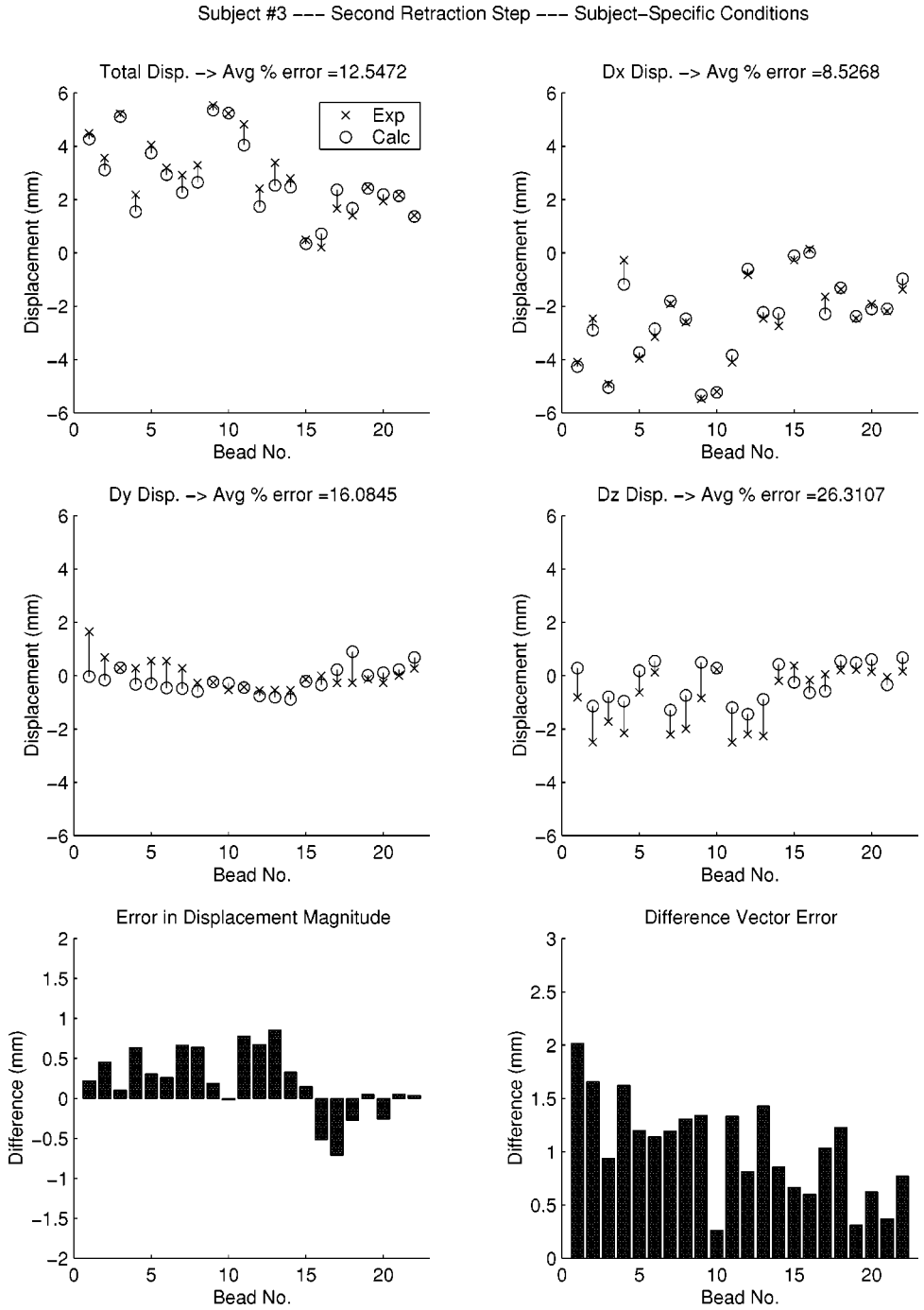

Fig. 8. Same as Fig. 6 with subject-specific boundary conditions in which case the average percent errors relative to the mean displacement magnitude, x displacement, y displacement, and z displacement have been reduced to 12%, 8%, 16%, and 26%, respectively. Similar reductions in the errors in displacement magnitude (bottom row, left) and difference vector magnitude (bottom row, right) are also found.

Hydrodynamically, both the anteriorly and posteriorly positioned sensors in the retracted hemisphere exhibit pressure spikes at the onset of retraction that decay to a steady level posteriorly which is elevated anteriorly for each successive retraction event. A clear pressure gradient exists antero–posterior in this hemisphere which increases with retractions. However, on the opposite side, pressure decreases initially for the first two retractions and rises toward baseline anteriorly while falling posteriorly during the relaxation period, but remains negative suggesting that the tissue in this hemisphere is under tension. The antero–posterior spatial gradient is similarly directed. Computationally, some of this overall behavior is present, although certain details are missing. Specifically, the spikes in the retracted hemisphere and even the initial dips in the contralateral side followed by transient decay (or rise) to an elevated steady-state is evident. The peak values are generally underpredicted and the decay rates are typically too slow. The transient dynamics are constrained by the numerical stability of the computational model which is inversely related to the square of the spatial discretization [41]. In the cases shown here, we were unable to increase the temporal resolution and concomitant pressure decay rate

TABLE III
CUMULATIVE AVERAGE AND MAX DISPLACEMENT ERRORS: MAGNITUDE (U) AND $x(U_x)$, $y(U_y)$, AND $z(U_z)$ DIRECTIONAL COMPONENTS IN MILLIMETERS FOR ALL FOUR SUBJECTS. STANDARD DEVIATIONS ($\pm$) ARE ALSO REPORTED FOR AVERAGED RESULTS

Retraction Step No.	U_x Error(mm) Average (Max)	U_y Error (mm) Average (Max)	U_z Error(mm) Average (Max)	U Error (mm) Average (Max)
1	0.3±0.3 (1.0)	0.4±0.3 (1.0)	0.3±0.2 (0.8)	0.3±0.3 (0.7)
2	0.5±0.4 (1.8)	0.5±0.4 (1.5)	0.4±0.3 (1.1)	0.4±0.5 (1.0)
3	0.7±0.7 (2.7)	0.7±0.5 (2.0)	0.5±0.4 (1.4)	0.6±0.7 (1.4)
4	1.0±0.9 (3.5)	1.1±0.9 (3.8)	0.7±0.6 (1.8)	0.9±1.0 (1.1)

TABLE IV
PER EVENT AVERAGE AND MAX DISPLACEMENT ERRORS: MAGNITUDE (U) AND x (U_x), y (U_y), AND z (U_z) DIRECTIONAL COMPONENTS IN MILLIMETERS FOR ALL FOUR SUBJECTS. STANDARD DEVIATIONS ($\pm$) ARE ALSO REPORTED FOR AVERAGED RESULTS

Retraction Step No.	U_x Error(mm) Average (Max)	U_y Error (mm) Average (Max)	U_z Error(mm) Average (Max)	U Error (mm) Average (Max)
2	0.3±0.2 (1.0)	0.3±0.2 (0.9)	0.3±0.2 (0.9)	0.3±0.3 (0.7)
3	0.3±0.2 (0.9)	0.3±0.2 (0.9)	0.3±0.2 (0.7)	0.3±0.3 (0.7)
4	0.3±0.4 (1.3)	0.5±0.5 (2.2)	0.3±0.3 (1.0)	0.3±0.5 (1.1)

TABLE V
PERCENT CAPTURE OF DEFORMATION: MAGNITUDE (U) AND CARTESIAN DIRECTIONS x (U_x), y (U_y), AND z (U_z)

Retraction Step No.	U_x	U_y	U_z	U
1	75.4	66.9	77.5	75.5
2	77.0	76.3	83.5	82.2
3	74.2	75.9	82.0	78.7
4	74.2	70.6	80.8	76.7

to better match the experimental time course without introducing numerical instabilities—the remedy for which would be increased mesh resolution. Nonetheless, the model appears to perform reasonably well in terms of the measured pressure behavior.

When subject-specific boundary conditions are applied there is clear improvement. For example, the x displacements of several beads with large errors (e.g., beads 2, and 4) and the y displacements overall which exhibit less negative (inferior) movement computationally are better matched. These gains were achieved by modifying the conditions around the edges of the craniotomy and near the base of the skull as described in the previous section. They served to reduce the overprediction of motion in the retraction and inferior (toward the brainstem) directions within the model.

Overall, the 75% (improved to 85% with individualized boundary conditions) motion compensation captured with the model is encouraging but likely not sufficient for neurosurgery, although it would clearly be better than relying only on preoperative images, which is often the case in practice. The dependence on individual boundary conditions to the level of 10%–20% may be expected. While we have not completed a formal sensitivity study, we have experimented with many more boundary condition options than reported here and consistently found variations in the resulting displacement fields on this order. This places the burden of deriving the data required to drive the computational model on the OR, for example, by tracking the position of the retractor blade. Intraoperative data may play another important role if also used to constrain the model, which, along with improvements in the underlying model, itself, will likely be the most productive avenues for achieving tissue motion estimates that are commensurate with the accuracy desired during neurosurgery.

V. CONCLUSION

A series of validation experiments for a computational model of tissue retraction have been completed *in vivo* using the porcine brain. Detailed measurements of tissue motion and interstitial pressure were compared to model calculations across a four subject set with each consisting of up to four separate retraction events. An incremental displacement formulation was employed which readily accommodated changes in retractor blade orientation during successive retractions. This improved the degree of data-model match by accounting for some of the geometric nonlinearity associated with sizable total deformation. Boundary conditions at the retractor blade surface pertaining to the hydrodynamical component of the model were also improved and found to be able to reasonably represent rather complex pressure dynamics which behaved quite differently in the two hemispheres. These advances bode well for the model and its ability to capture tissue deformation from complicated surgical procedures such as retraction. Certainly, the 75%–80% motion recapture rate found in these experiments would constitute a significant improvement over not using any form of tissue motion compensation in the OR.

With subject-specific boundary conditions error can be reduced even further, typically 10% or more, at least in the experiments reported here. This suggests that there are aspects of the physical motion which require additional study. While overall there was a considerable amount of consistency across the experiments performed in each subject, some individualized behavior is not unexpected. For example, there was variation in brain volume and retractor blade location (in particular, depth of insertion) that may play a role in the unaccounted data-model match discrepancies. Future experiments could well benefit from MR imaging of the brain under retraction where higher definition of the parenchyma could be exploited to improve our understanding of how the cortical surface is moving both in and around the craniotomy and near the brain stem where we found tailored boundary conditions can make a difference.

Additional retraction experiments with tissue motion lateral to medial and anterior to posterior are also warranted. These would create other interactions between the cranium and tissue

at the closed and open surfaces that should be captured with the model. However, relative to a lateral to medial retraction, the experiments reported here are more complex in that the two hemispheres experience different types of loading conditions. Lateral to medial retraction would leave both hemispheres essentially in compression much like our previously reported piston translation studies; hence, we would expect to observe a high degree of data-model agreement in this configuration. The pressure response remains an element of the system which has not been fully characterized. While the general model behavior emulates that observed in the porcine brain, we exploited the calibration curve generated during the piston translation study to drive the pressure conditions associated with the retractor blade displacement, although we did so through a more realistic boundary relationship involving a coupling coefficient rather than directly enforcing a pressure value at the tissue-blade interface as before. Nonetheless, we might expect improved model performance with better empirically derived pressure calibration as a function of blade displacement by using an instrumented retractor with pressure sensing capabilities in the future.

REFERENCES

[1] T. Peters, B. Davey, P. Munger, R. Comeau, A. Evans, and A. Olivier, "Three-dimensional multimodal image-guidance for neurosurgery," *IEEE Trans. Med. Imag.g*, vol. 15, pp. 121–128, Apr. 1996.

[2] W. E. L. Grimson, G. J. Ettlinger, S. J. White, T. Lozano-Perez, W. M. Wells, 3rd, and R. Kikinis, "An automated registration method for frameless stereotaxy, image guided surgery and enhanced reality visualization," *IEEE Trans. Med. Imag.*, vol. 15, pp. 129–140, Apr. 1996.

[3] D. W. Roberts, J. W. Strohbehn, J. F. Hatch, W. Murray, and H. Kettenberger, "A frameless stereotactic integration of computerized tomographic imaging and the operating microscope," *J. Neurosurg.*, vol. 65, pp. 545–549, 1986.

[4] R. L. Galloway, Jr., R. J. Maciunas, and C. A. Edwards, "Interactive image-guided neurosurgery," *IEEE Trans. Biomed. Eng.*, vol. 39, pp. 1226–1231, May 1992.

[5] G. H. Barnett, D. W. Kormos, C. P. Steiner, and J. Weisenberger, "Intraoperative localization using an armless, frameless stereotactic wand," *Neurosurgery*, vol. 33, pp. 674–678, 1993.

[6] D. R. Sanderman and S. S. Gill, "The impact of interactive image guided surgery: The Bristol experience with the ISF/Elekta viewing wand," *Acta Neurochirurgica, Suppl.*, vol. 64, pp. 54–58, 1995.

[7] T. L. Lewis, R. L. Galloway, and S. Schreiner, "An ultrasonic approach to localization of fiducial markers for interactive, image-guided neurosurgery—Part I: Principles," *IEEE Trans. Biomed. Eng.*, vol. 45, pp. 620–630, May 1998.

[8] K. R. Smith, K. J. Frank, and R. D. Bucholz, "The NeuroStation—A highly accurate, minimally invasive solution to frameless stereotactic neurosurgery," *Comput. Med. Imag. Graph.*, vol. 18, pp. 247–256, 1994.

[9] H. Dickhaus, K. Ganser, A. Staubert, M. M. Bonsanto, C. R. Wirtz, V. M. Tronnier, and S. Kunze, "Quantification of brain shift effects by MR-imaging," in *Proc. 19th Annu. Int. Conf. IEEE Engineering in Medicine and Biology Society*, 1997, pp. 491–494.

[10] D. W. Roberts, A. Hartov, F. E. Kennedy, M. I. Miga, and K. D. Paulsen, "Intraoperative brain shift and deformation: A quantitative clinical analysis of cortical displacements in 28 cases," *Neurosurgery*, vol. 43, no. 4, pp. 749–760, 1998.

[11] D. L. G. Hill, C. R. Maurer, R. J. Maciunas, J. A. Barwise, J. M. Fitzpatrick, and M. Y. Wang, "Measurement of intraoperative brain surface deformation under a craniotomy," *Neurosurgery*, vol. 43, no. 3, pp. 514–528, 1998.

[12] N. L. Dorward, A. Olaf, B. Velani, F. A. Gerritsen, W. F. J. Harkness, N. D. Kitchen, and D. G. T. Thomas, "Postimaging brain distortion: Magnitude, correlates, and impact on neuronavigation," *J. Neurosurg.*, vol. 88, pp. 656–662, 1998.

[13] C. R. Maurer, D. L. G. Hill, A. J. Martin, H. Liu, M. McCue, D. Rueckert, D. Lloret, W. A. Hall, R. E. Maxwell, D. J. Hawkes, and C. L. Truwit, "Investigation of interoperative brain deformation using a 1.5-T interventional mr system: Preliminary results," *IEEE Trans. Med. Imag.*, vol. 17, pp. 817–825, Oct. 1998.

[14] A. Nabavi, P. McL. Black, D. T. Gering, C. Westin, V. Mehta, R. S. Pergolizzi, M. Ferrant, S. K. Warfield, N. Hata, R. B. Schwartz, W. M. Wells, R. Kikinis, and F. A. Jolesz, "Serial intraoperative magnetic resonance imaging of brain shift," *Neurosurgery*, vol. 48, pp. 787–798, 2001.

[15] S. K. Warfield, A. Nabavi, T. Butz, K. Tuncali, S. G. Silverman, P. McL. Black, F. A. Jolesz, and R. Kikinis, "Intraoperative segmentation and nonrigid registration for image guided therapy," in *Lecture Notes in Computer Science*. Berlin, Germany: Springer-Verlag, 2000, vol. 1935, Medical Image Computing and Computer-Assisted Intervention—MICCAI'00, pp. 176–185.

[16] D. W. Roberts, M. I. Miga, F. E. Kennedy, A. Hartov, and K. D. Paulsen, "Intraoperatively updated neuroimaging using brain modeling and sparse data," *Neurosurgery*, vol. 45, no. 5, pp. 1199–1207, 1999.

[17] P. J. Edwards, D. L. G. Hill, J. A. Little, and D. J. Hawkes, "Deformation for image-guided interventions using a three component tissue model," in *Lecture Notes in Computer Science*, Duncan and Gindi, Eds. Berlin, Germany: Springer-Verlag, 1997, vol. 15th International Conference for Information Processing in Medical Imaging, pp. 218–231.

[18] O. Skrinjar, D. Spencer, and J. Duncan, "Brain shift modeling for use in neurosurgery," in *Lecture Notes in Computer Science*. Berlin, Germany: Springer-Verlag, 1998, vol. 1496, Medical Image Computing and Computer-Assisted Intervention—MICCAI'98, pp. 1067–1074.

[19] S. K. Kyriacou and C. Davatzikos, "A biomechanical model of soft tissue deformation, with applications to nonrigid registration of brain images with tumor pathology," in *Lecture Notes in Computer Science*. Berlin, Germany: Springer-Verlag, 1998, vol. 1496, Medical Image Computing and Computer-Assisted Intervention—MICCAI'98, pp. 531–538.

[20] M. Ferrant, S. K. Warfield, A. Nabavi, F. A. Jolesz, and R. Kikinis, "Registration of 3d intraoperative mr images of the brain using a finite element biomechanical model," *IEEE Trans. Med. Imag.*, vol. 20, pp. 1384–1397, Dec. 2001.

[21] A. D. Castellano-Smith, T. Hartkens, J. Schnabel, D. R. Hose, H. Liu, W. A. Hall,, C. L. Truwit, D. J. Hawkes, and D. L. G. Hill, "Constructing patient specific models for correcting intraoperative brain deformation," in *Lecture Notes in Computer Science*, vol. 2208, Medical Image Computing and Computer-Assisted Intervention—MICCAI'01. Berlin, Germany, 2001, pp. 1091–1098.

[22] A. Hagemann, K. Rohr, H. S. Stiehl, U. Spetzger, and J. M. Gilsbach, "Biomechanical modeling of the human head for physically based, nonrigid image registration," *IEEE Trans. Med. Imag.*, vol. 18, pp. 875–884, Oct. 1999.

[23] S. K. Warfield, M. Ferrant, X. Gallez, A. Nabavi, F. A. Jolesz, and R. Kikinis, "Real-time biomechanical simulation of volumetric brain deformation for image guided neurosurgery," in *Proc. High Performance Networking and Computing Conf.*, vol. 230, 2000, pp. 1–16.

[24] M. Ferrant, A. Nabavi, B. Macq, R. Kikinis, and S. K. Warfield, "Real-time simulation and visualization of volumetric brain deformation for image guided neurosurgery," *Proc. SPIE*, vol. 4319, pp. 366–373, 2001.

[25] K. Miller, "Constitutive model of brain tissue suitable for finite element analysis of surgical procedures," *J. Biomech.*, vol. 32, pp. 531–537, 1999.

[26] M. I. Miga, K. D. Paulsen, P. J. Hoopes, F. E. Kennedy, A. Hartov, and D. W. Roberts, "*In vivo* modeling of interstitial pressure in the brain under surgical load using finite elements," *ASME J. Biomech. Eng.*, vol. 122, pp. 354–363, 2000.

[27] M. I. Miga, "Development and quantification of a 3D brain deformation model for model-updated image-guided stereotactic neurosurgery," Ph.D. dissertation, Dartmouth College, Thayer School Eng., Hanover, NH, 1998.

[28] M. I. Miga, D. W. Roberts, F. E. Kennedy, L. A. Platenik, A. Hartov, K. E. Lunn, and K. D. Paulsen, "Modeling of retraction and resection for intraoperative updating of images during surgery," *Neurosurgery*, vol. 49, pp. 75–85, 2001.

[29] T. Nagashima, N. Tamaki, M. Takada, and Y. Tada, "Formation and resolution of brain edema associated with brain tumors. A comprehensive theoretical model and clinical analysis," *Acta Neurochirurgica, Suppl.*, vol. 60, pp. 165–167, 1994.

[30] P. J. Basser, "Interstitial pressure, volume, and flow during infusion into brain tissue," *Microvasc. Res.*, vol. 44, pp. 143–165, 1992.

[31] K. Miller, K. Chinzei, G. Orssengo, and P. Bednarz, "Mechanical properties of brain tissue *in-vivo*: Experiment and computer simulation," *J. Biomech.*, vol. 33, pp. 1369–1376, 2000.

[32] M. A. Biot, "General theory of three-dimensional consolidation," *J. Appl. Phys.*, vol. 12, pp. 155–164, 1941.

[33] K. D. Paulsen, M. I. Miga, F. E. Kennedy, P. J. Hoopes, A. Hartov, and D. W. Roberts, "A computational model for tracking subsurface tissue deformation during stereotactic neurosurgery," *IEEE Trans. Biomed. Eng.*, vol. 46, pp. 213–225, Feb. 1999.

[34] S. Hakim, J. G. Venegas, and J. D. Burton, "The physics of the cranial cavity, hydrocephalus and normal pressure hydrocephalus: Mechanical interpretation and mathematical model," *Surg. Neurol.*, vol. 5, pp. 187–210, 1976.

[35] K. Miller, "Modeling soft tissue using biphasic theory—A word of caution," *Comput. Meth. Biomech. Biomed. Eng.*, vol. 1, pp. 261–263, 1998.

[36] L. A. Platenik, M. I. Miga, F. E. Kennedy, D. W. Roberts, A. Hartov, K. E. Lunn, and K. D. Paulsen, "*In vivo* comparison of an incremental versus single-step retraction model for intraoperative compensation," *Proc. SPIE*, vol. 4319, pp. 358–365, 2001.

[37] M. A. Howard, III, B. A. Abkes, M. C. Ollendieck, M. D. Noh, R. C. Ritter, and G. T. Gillies, "Measurement of the force required to move a neurosurgical probe through *in vivo* human brain tissue," *IEEE Trans. Biomed. Eng.*, vol. 46, pp. 891–894, July 1999.

[38] T. Koyama, H. Okudera, and S. Kobayashi, "Computer-generated surgical simulation of morphological changes in microstructures: Concepts of 'virtual retractor'," *Neurosurgery*, vol. 46, no. 1, pp. 118–135, 2000.

[39] J. M. Sullivan Jr., G. Charron, and K. D. Paulsen, "A three dimensional mesh generator for arbitrary multiple material domains," *Finite Element Anal. Design*, vol. 25, pp. 219–241, 1997.

[40] M. I. Miga, K. D. Paulsen, F. E. Kennedy, P. J. Hoopes, A. Hartov, and D. W. Roberts, "*In vivo* analysis of heterogeous brain deformation computations for model-updated image guidance," *Comput. Meth. Biomech. Biomed. Eng.*, vol. 3, pp. 129–146, 2000.

[41] M. I. Miga, K. D. Paulsen, and F. E. Kennedy, "Von Neumann stability analysis of Biot's general two-dimensional theory of consolidation," *Int. J. Numer. Methods Eng.*, vol. 43, pp. 955–974, 1998.

Leah A. Platenik received the B.S. degree in biomedical engineering with an electrical concentration from Rensselear Polytechnic Institute, Troy, NY. She received the M.S. degree from the Thayer School of Engineering, Dartmouth College, Hanover, N.H. in 2001.

She is currently employed as an Associate Staff Scientist at Massachusetts Institute of Technology Lincoln Lab.

Michael I. Miga received the B.S., M.S. degrees in mechanical engineering at the University of Rhode Island, Kingston, in 1992, and 1994, respectively. He received his Ph.D. degree from Dartmouth College, Hanover, NH, in 1998, concentrating in biomedical engineering.

Following his doctoral work, he continued on at Dartmouth as a Postdoctoral Research Associate and later Research Assistant Professor until fall of 2000. He is currently an Assistant Professor in the Department of Biomedical Engineering, Vanderbilt University, Nashville, TN. His research interests include computational modeling in biomedicine, model-updated image guided surgery, inverse problems, tissue, and biofluid mechanics.

David W. Roberts received the A.B. degree from Princeton University, Princeton, NJ, the M.A. degree from Oxford University, Oxford, U.K. and the M.D. degree from Dartmouth Medical School, Hanover, NH.

He is Professor of Surgery (Neurosurgery) at Dartmouth Medical School and Chairman of Neurosurgery at the Dartmouth-Hithcock Medical Center. His research interests are in the areas of frameless stereotaxy and intractable epilepsy.

Dr. Roberts is President of the American Society of Stereotactic and Functional Neurosurgery.

Karen E. Lunn received the A.B. degree in physics and philosophy from Bowdoin College, Brunswick, ME, in 1998. She received the M.S. degree in biomedical engineering from the Thayer School of Engineering at Dartmouth College, Hanover, NH, in 2001. She is currently working towards the Ph.D. degree in biomedical engineering at Dartmouth College. Her thesis work involves the integration of measured displacement data with a brain deformation model.

For the 1998-1999 school year, she taught physics and mathematics to high school students at Verde Valley School in Sedona, AZ.

Francis E. Kennedy received the B.S. degree from Worcester Polytechnic Institute, Worcester, MA, in 1963 and the M.S. degree from Stanford University, Stanford, CA, in 1965, both in mechanical engineering. He received the Ph.D. degree in mechanics from Rensselaer Polytechnic Institute Troy. NY, in 1973.

Since 1974, he has been on the faculty of Thayer School of Engineering at Dartmouth College, Hanover, NH. where he is now Professor of Engineering. His research activity has been in the following areas: biomechanics, tribology, experimental and numerical methods in contact mechanics, biomechanics, and heat transfer. He is the author or co-author of more than 80 technical papers and four book chapters and has edited four books (symposium volumes). He was Chief Technical Editor of the ASME Journal of Tribology (1993-1998).

Alex Hartov received the BSEE degree with high honors from Northeastern University, Boston, MA, in 1984. He received the M.S. degree in medical imaging and 3-D reconstruction in 1988 and the Ph.D. degree in intraoperative ultrasound hyperthermia in 1991, both from the Thayer School of Engineering, Hanover, NH.

He spent six years as an Electronics Design Engineer while in school and after. He is currently Research Assistant Professor at the Dartmouth Medical School and the Thayer School of Engineering. His current projects and interests are in brain deformation, electrical impedance spectroscopy, microwave imaging, coronary artery stress distribution, and prostate hyperthermia. He is a part time consultant in biomedical related projects.

Keith D. Paulsen (S'85–M'86) received the B.S. degree in biomedical engineering from Duke University, Durham, NC, in 1981 and the M.S. and Ph.D. degrees in biomedical engineering from Dartmouth College, Hanover, NH, in 1984 and 1986, respectively.

From 1986 to 1988, he was an Assistant Professor in the Electromagnetics Group within the Department of Electrical and Computer Engineering, University of Arizona, Tucson. He is currently a Professor at the Thayer School of Engineering, Dartmouth College and the Director of the Radiobiology and Bioengineering Research Program for the Norris Cotton Cancer Center within the Dartmouth-Hitchcock Medical Center, Lebanon, NH. His research interests include computational methods with particular emphasis on biomedical problems in cancer therapy and imaging, and model-guided surgery.